

# CO<sub>2</sub> hydrogenation to C<sub>5+</sub> hydrocarbons over K-promoted Fe/CNT catalyst: Effect of potassium on structure–activity relationship

Liya Dai  | Yao Chen  | Renjie Liu  | Xin Li  | Niamat Ullah  | Zhenhua Li 

School of Chemical Engineering and Technology, Tianjin University, Tianjin, China

## Correspondence

Zhenhua Li, School of Chemical Engineering and Technology, Tianjin University, Yaguan Road 135, Tianjin 300350, China.  
Email: zhenhua@tju.edu.cn

## Funding information

Joint Funds of the National Natural Science Foundation of China, Grant/Award Number: U20A20124; Program of Introducing Talents of Discipline to Universities, Grant/Award Number: BP0618007

Developing efficient catalysts for direct CO<sub>2</sub> hydrogenation to fuel hydrocarbons is of great significance for the effective utilization of CO<sub>2</sub>, and C<sub>5+</sub> selectivity is one critical indicator for the process economics. In this work, a series of K-promoted Fe/CNT catalysts were prepared by the co-impregnation method, and their catalytic performance for CO<sub>2</sub> hydrogenation was studied in a slurry-bed reactor. As a result, CO<sub>2</sub> conversion and C<sub>5+</sub> selectivity showed positive correlation with the increase of K/Fe ratio from 0 to 0.3, but further increase of K/Fe ratio above 0.3 slightly affected its. The catalyst with a K/Fe molar ratio of 0.3 achieved the best performance with CO<sub>2</sub> conversion of 23.7% and C<sub>5+</sub> selectivity of 56%. In addition, the structure–activity relationship of the catalyst was discussed based on various characterization results. K-modified catalysts presented a higher specific surface area and stronger CO<sub>2</sub> chemisorption, which helped to improve CO<sub>2</sub> conversion and C<sub>5+</sub> selectivity. However, excessive potassium loading caused a loss of specific surface area, reduction degree, and graphitization degree of the catalyst, which inhibited the CO<sub>2</sub> chemisorption and the formation of C<sub>5+</sub> hydrocarbons.

## KEYWORDS

C<sub>5+</sub> hydrocarbons, CO<sub>2</sub> hydrogenation, iron catalyst, potassium

## 1 | INTRODUCTION

The continuous increase of CO<sub>2</sub> emissions caused by the massive use of fossil fuels has led to a runaway greenhouse effect.<sup>[1]</sup> It is urgent to find effective ways to reduce CO<sub>2</sub> emissions because the world's dependence on fossil fuels will not decline for a long time. A valid method to reduce CO<sub>2</sub> emissions is carbon capture and storage (CCS) technology, which has been well studied in recent years.<sup>[2,3]</sup> Another technology is carbon capture and utilization (CCU), which can convert CO<sub>2</sub> into fuels and

other valuable chemicals, provides an efficient strategy to cycle the carbon, and has economic benefits.<sup>[4–6]</sup> Among them, the reaction of CO<sub>2</sub> hydrogenation to long-chain hydrocarbon has aroused widespread concern because the broad market of these products would significantly reduce CO<sub>2</sub> emission and realize the effective utilization of carbon resources.<sup>[7–9]</sup> Owing to the thermodynamic stability of CO<sub>2</sub>, the development of high-efficiency catalysts for this process is the pivotally technical bottleneck. CO<sub>2</sub> can be directly hydrogenated into hydrocarbons by modified CO<sub>2</sub> Fischer–Tropsch synthesis (CO<sub>2</sub>-FTS) process. This process included two sequential reactions, in which CO<sub>2</sub> was first reduced to CO via the reverse water–

Liya Dai and Yao Chen contribute equally to this work.

gas shift (RWGS) reaction and then CO was hydrogenated to hydrocarbons through Fischer–Tropsch synthesis (FTS) reaction.<sup>[10,11]</sup> Therefore, CO<sub>2</sub> hydrogenation to long-chain hydrocarbons by the CO<sub>2</sub>-FTS process required resultful catalysts with active sites of both RWGS and FTS reaction.

Relative to other metals in VIII group,<sup>[12–14]</sup> only Fe-based catalysts presented excellent catalytic ability for RWGS and FTS processes and had low CH<sub>4</sub> selectivity at high temperature,<sup>[15,16]</sup> so they were preferred for modified CO<sub>2</sub>-FTS reaction. Furthermore, it was reported that Fe<sub>3</sub>O<sub>4</sub> was very capable of activating CO<sub>2</sub> and iron carbide was effective for enhancing chain growth. However, to obtain better CO<sub>2</sub> conversion and higher selectivity to desired hydrocarbons, the significant impact of supports and additives on the performance of catalyst should also be concerned.<sup>[17,18]</sup> Metal oxides were widely used to support Fe-based catalysts for CO<sub>2</sub> hydrogenation. For example, Al<sub>2</sub>O<sub>3</sub> had an excellent performance in terms of CO<sub>2</sub> conversion and light hydrocarbon selectivity.<sup>[19,20]</sup> Boreriboon et al.<sup>[21]</sup> compared the CO<sub>2</sub> hydrogenation performance of monometallic and bimetallic catalysts supported on TiO<sub>2</sub>, who found that Fe/TiO<sub>2</sub> catalyst had low selectivity to higher hydrocarbons and Co/TiO<sub>2</sub> and Cu/TiO<sub>2</sub> catalysts only produced CH<sub>4</sub> and CO. Further studies certificated that the strong interaction between iron and metallic oxide support inhibited the reduction and carbonization of iron,<sup>[8]</sup> thus restraining the activation of CO<sub>2</sub> and the generation of long-chain hydrocarbons. Chew et al.<sup>[22]</sup> found that interaction between iron oxide and silica was much stronger, thus inhibiting the reduction of iron species. As a result, the activity of Fe/NCNT catalyst for CO<sub>2</sub> hydrogenation was almost twice than Fe/SiO<sub>2</sub> catalyst. Zeolite was usually used in the synthesis of light olefins and hydrocracking reaction. In some modified zeolite, oligomerization was inhibited due to the reduction of acid sites, which promoted the production of light olefins at the expense of long-chain hydrocarbons.<sup>[23–25]</sup> And the channel in ZSM-5 and mordenite might hinder the diffusion of long-chain hydrocarbons.<sup>[26]</sup> The carbon materials with weak metal-carrier interaction endowed the iron-based catalysts with the favorable ability to active iron species into iron carbides, so it has been regarded as an excellent support for CO<sub>2</sub> hydrogenation.<sup>[27–30]</sup> Compared with other carbon materials, using carbon nanotubes (CNTs) as the support promoted the iron–carbon interaction on the curved surface of CNTs,<sup>[31]</sup> thereby avoiding the generation of irreducible iron species and showing remarkable C<sub>5+</sub> selectivity in FTS reaction.<sup>[27,32]</sup> And the long-range ordered structure of CNTs is conducive to the aggregation of the reaction intermediate.<sup>[33]</sup> CO<sub>2</sub> hydrogenation reaction using N-doped CNT support was beneficial to CO<sub>2</sub>

conversion due to the higher iron dispersion and better reducibility,<sup>[22]</sup> but it also gave rise to high selectivity of methane because of the high H<sub>2</sub>/CO ratio adsorbed by some active sites on the Fe/NCNT catalyst surface.<sup>[34]</sup> Therefore, it is necessary to change the surface adsorption capacity of the catalyst by adding promoters to adjust the product distribution.

Alkali metal ions were acknowledged as common electronic auxiliaries in Fe-based catalysts, which were assumed to increase the surface alkalinity of the catalysts and restrain the chemisorption of H<sub>2</sub>, thus facilitating CO and CO<sub>2</sub> chemisorption and chain-growth probability.<sup>[35,36]</sup> Xiong et al.<sup>[37]</sup> proved that the Fe/CNT catalysts promoted by potassium and sodium not only suppressed the production of methane but also increased the distribution of olefins and selectivity of C<sub>5+</sub> in FTS reaction. You et al.<sup>[38]</sup> found that adding alkali metals to non-supported Fe-based catalysts could significantly improve the CO<sub>2</sub> conversion and C<sub>5+</sub> selectivity. Specifically, the catalysts modified by K and Rb achieved better performance. Besides, potassium could promote the carbonization of iron species, which was one of the key factors for the low methane selectivity and high chain-growth probability in CO<sub>x</sub> hydrogenation reaction.<sup>[39,40]</sup>

Until now, few studies on the mechanism of K-modified Fe-based catalyst for CO<sub>2</sub> hydrogenation reaction were reported, and the effect of K on the selectivity of long-chain hydrocarbons remained unclear. In this work, a series of Fe-xK/CNT catalysts with different contents of potassium were prepared by co-impregnation on both acid/alkali-treated CNTs, and their catalytic performance for CO<sub>2</sub> hydrogenation was tested in a slurry-bed reactor. The influence of K-doping on the structure and property of the catalysts was investigated through various characterization techniques to clarify the role of K and the structure–activity relationship.

## 2 | EXPERIMENTAL

### 2.1 | Catalyst preparation

To remove the amorphous carbon and obtain the oxygen-functionalized CNTs, commercial CNTs were pretreated with nitric acid (65 wt.%) at 120 °C for 6 h. After cooling down to room temperature, the mixture was diluted with water. The CNTs were filtered out and washed with deionized water to neutrality and then dried it at 110 °C for 12 h. Afterward, the acid-treated CNTs were mixed evenly with the KOH solution (7.5 M). The mixture was placed in a Teflon cup and heated at 190 °C for 10 h. After cooling down, the sample was washed with water

so to reach a pH value of 7 and then dried at 110 °C overnight.

Iron-based catalysts were prepared by an impregnation method using ferric nitrate ( $\text{Fe}(\text{NO}_3)_3 \cdot 9\text{H}_2\text{O}$ ) as the iron precursor. The weight of solvent should be determined by measuring the saturated adsorption capacity of the carrier before preparing the catalyst. The treated CNTs were immersed in the aqueous solution of ferric nitrate aiming at a theoretical Fe loading of 20 wt.%. The mixture was placed in a rotary evaporator at 80 °C for 2 h and then placed in a vacuum drying oven at 110 °C for 12 h. Finally, the solid product was calcined at 400 °C with a heating rate of 2 °C/min for 5 h in Ar atmosphere, and the obtained sample was labeled as Fe/CNT catalyst. The preparation method of the K-modified catalysts is as follows: Five kinds of aqueous solution with different molar ratios of K and Fe ( $n(\text{K})/n(\text{Fe}) = 0.05, 0.15, 0.3, 0.6, 1$ ) were dropped in the processed CNTs, and the subsequent treatment was the same as that of Fe/CNT catalyst. The obtained catalysts were named as Fe- $x\text{K}$ /CNTs, where  $x$  was the molar ratio of  $n(\text{K})/n(\text{Fe})$ , including 0.05, 0.15, 0.3, 0.6, and 1.

## 2.2 | Catalyst characterization

$\text{N}_2$  adsorption–desorption was tested on a Micromeritics TriStar 3000 physical adsorb instrument. A 200 mg sample was degassed at 300 °C for 4 h, determining the amount of adsorbed nitrogen under  $-196$  °C. The calculations of surface area and pore size distribution were dependent on the BET equation and BJH method, respectively.

The calcined catalysts were subjected to phase analysis and qualitative analysis by the Rigaku D/Max-2500v/pc X-ray diffractometer with Cu/ $\text{K}\alpha$  source. The scanning range of spectra was  $2\theta = 5\text{--}85^\circ$ , and the accelerating voltage was 40 kV. The crystallite phases were identified by comparing the diffraction peaks with the JCPDS cards, and the average size of the  $\text{Fe}_2\text{O}_3$  crystallites in the calcined catalysts was estimated using the Scherrer equation.

The morphology of the catalyst was observed by transmission electron microscope (JEM-2100F) at 200 kV, and the element mapping of the catalyst was analyzed by JEM-F200.

Catalyst reducibility was measured on the AutoChem 2910 automatic chemical adsorption instrument. A 50 mg sample was first purged with argon at 200 °C for 60 min and then cooled to 50 °C. The flow was switched to 10%  $\text{H}_2$ –90% Ar gas, and the reactor was heated from 50 to 900 °C with a heating rate of 10 °C/min. The hydrogen

consumption signal was detected by the thermal conductivity detector (TCD).

The elemental surface analysis of the calcined catalysts was measured on the PHI 1600 ESCA X-ray photoelectron spectrometer (XPS) using Mg/ $\text{K}\alpha$  radiation (1253.3 eV) as the X-ray source. The pressure of the sample chamber was  $1.2 \times 10^{-8}$  Torr, and calibrating the binding energy (BE) of the adventitious carbon at 284.8 eV was used as a reference.

$\text{CO}_2$  temperature-programmed desorption ( $\text{CO}_2$ -TPD) was conducted in the same equipment as the  $\text{H}_2$ -TPR. The catalyst was reduced with  $\text{H}_2$  at 300 °C, then switched the gas to argon, and purged sample for 1 h. After prereduction, the gas was switched to helium and purged the sample until the baseline was stable. Pulsed  $\text{CO}_2$  in multiple time and then purged He for 30 min to remove the physically adsorbed  $\text{CO}_2$  on the catalyst surface. Finally, the reactor was heated to 500 °C at a rate of 10 °C/min, during which  $\text{CO}_2$  desorption signals were recorded with TCD.

The thermal stability of the catalysts was subjected to thermogravimetric analysis using STA 449 F3 and NETZSCH system. The catalyst was heated in air (50 mL/min) from ambient temperature to 800 °C at 10 °C/min.

The catalyst was first ground into a powder and then investigated the structural stability by a DXR laser Raman spectrometer with a laser wavelength of 532 nm and a slit width of 25  $\mu\text{m}$  under the laser discharged by Spectra Physics 2020 argon ion.

## 2.3 | Catalytic activity test for $\text{CO}_2$ hydrogenation

The activity for  $\text{CO}_2$  hydrogenation on the catalyst was carried out using a slurry-bed reactor. Before active test, 8.3 g of calcined catalyst was activated ex situ in a plug flow reactor using 25% $\text{H}_2$ /He at 350 °C for 10 h. Then, the reduced catalyst mixed with melted Polywax 3000 was put into the slurry reactor. The catalyst was further reduced in  $\text{H}_2$  at 300 °C for 24 h, and the other reaction conditions were as follows: The reaction temperature was controlled at a range of 300 °C, the reaction pressure was 2 MPa, and the reaction gas was the mixture of  $\text{H}_2$  and  $\text{CO}_2$  (molar ratio:  $\text{H}_2/\text{CO}_2 = 3$ ), and the space velocity was 4.0 L/g (cat)-h. The gaseous products were reduced to atmospheric pressure and then introduced into an online gas chromatography (Agilent 6820) equipped with a TCD and a flame ionization detector (FID) by using He as the carrier gas. The collected hydrocarbon (oil + wax) phases were analyzed offline by using a gas

chromatograph SP-3420 equipped with FID detector using a HP-5 capillary column.

The conversion of CO<sub>2</sub> and selectivity of hydrocarbons are defined as follows:

$$\text{CO}_2 \text{ conversion rate (\%)} = (F_{\text{CO}_2,\text{in}} - F_{\text{CO}_2,\text{out}}) / F_{\text{CO}_2,\text{in}} \times 100 \quad (1)$$

$$C_n \text{ selectivity (S}_n, C_n \%, n = 1, 2, 3, 4) = \frac{nF_{\text{An}}}{(F_{\text{CO}_2,\text{in}} - F_{\text{CO}_2,\text{out}} - F_{\text{CO},\text{out}})} \times 100 \quad (2)$$

$$C_{5+} \text{ hydrocarbons selectivity (S}_{5+}, C_{5+} \%) = 100 - \sum_{n=1}^4 S_n \quad (3)$$

where  $F_{\text{CO}_2,\text{in}}$  and  $F_{\text{CO}_2,\text{out}}$  are the molar flow rate of CO<sub>2</sub> at inlet and outlet,  $F_{\text{CO},\text{out}}$  is the molar flow rate of outlet CO,  $n$  is the carbon number, and  $F_{\text{An}}$  is the molar flow rate of the hydrocarbon An.

### 3 | RESULTS AND DISCUSSION

#### 3.1 | Phase structure of the catalysts

The amount of potassium also affects the textural properties of catalysts. The XRD patterns, shown in Figure 1, point that  $\alpha\text{-Fe}_2\text{O}_3$  (JCPDS: PDF#33-0664) is the main crystalline phase in all catalysts with several diffraction peaks emerging at  $2\theta = 24.3^\circ, 33.4^\circ, 35.9^\circ, 49.8^\circ, 54.5^\circ,$

$62.9^\circ,$  and  $64.5^\circ$ . The sharper diffraction peaks of  $\alpha\text{-Fe}_2\text{O}_3$  in the unmodified catalyst mean that it has a larger grain size than the K-modified catalysts. As listed in Table 1, the average crystallite size calculated from the diffraction peak at  $35.9^\circ$  by the Scherrer equation decreases from 25.6 to 19.1 nm with the increase of K content. In addition, some  $\text{Fe}_3\text{O}_4$  (JCPDS: PDF#75-0449) was detected at  $2\theta = 30.4^\circ, 35.8^\circ,$  and  $67.2^\circ,$  and a few  $\chi\text{-Fe}_5\text{C}_2$  (JCPDS: PDF#89-2544) was also discovered around  $45^\circ,$  which were generated via a reduction reaction between CNTs and  $\alpha\text{-Fe}_2\text{O}_3$  during the calcination process of the catalysts.

TEM images shown in Figure 2 indicate that some iron particles are located inside the CNT tubes. The average grain size obtained by TEM decreases with the K adding, which is similar with the results in XRD. These estimates correspond well with the finding that K inhibited the growth of Fe particles. The STEM images and the corresponding EDX mapping images in Figure 2 reveal the distribution of Fe and K over the CNT support. It is clear that most of K is dispersed uniformly on the Fe species with a small amount K being scattered on the CNT support.

#### 3.2 | Morphological properties of the catalysts

N<sub>2</sub> adsorption–desorption isotherms and pore size distribution of the Fe-xK/CNT catalysts with different potassium loadings are presented in Figure 3, and their

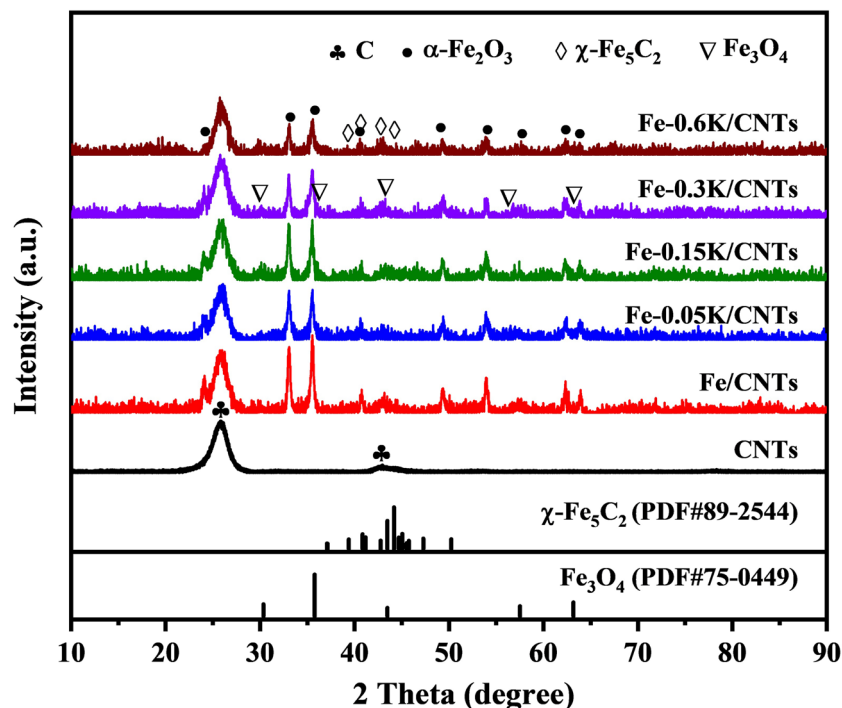


FIGURE 1 XRD patterns of calcined catalysts and support

TABLE 1 Morphological properties and amounts of CO<sub>2</sub> chemisorption for fresh catalysts and support

Sample	Specific surface area <sup>a</sup> (m <sup>2</sup> /g)	Pore volume <sup>b</sup> (cm <sup>3</sup> /g)	Average pore diameter <sup>c</sup> (nm)	Fe <sub>2</sub> O <sub>3</sub> particle size <sup>d</sup> (nm)	CO <sub>2</sub> adsorption <sup>e</sup> (μmol/g)
CNTs	159.8	0.90	22.6	----	----
Fe/CNTs	152.4	0.63	17.1	25.6	250.3
Fe-0.05K/ CNTs	177.1	0.61	14.3	22.2	316.5
Fe-0.15K/ CNTs	156.1	0.62	16.3	20.8	267.0
Fe-0.3K/ CNTs	157.6	0.60	15.6	19.5	261.0
Fe-0.6K/ CNTs	156.2	0.58	15.2	19.1	205.4

<sup>a</sup>Specific surface area was calculated by BET method.

<sup>b</sup>Pore volume adsorbed at p/p<sub>0</sub> = 0.99.

<sup>c</sup>Average pore diameter was determined by the BJH method.

<sup>d</sup>Estimated from the Scherrer equation of corrected 2θ position.

<sup>e</sup>CO<sub>2</sub> adsorption capacity was calculated from CO<sub>2</sub>-TPD profile.

morphological properties are listed in Table 1. It can be seen from Figure 3a that the five catalysts and support all represent typical IV-type N<sub>2</sub> adsorption isotherm with the H4-type hysteresis loop, which have no obvious saturated adsorption platform. These results indicate that the pore structure in catalysts was irregular and the catalysts had a mixture of mesopores and micropores. The pore distribution curves of all samples (Figure 3b) are similar in a wide range of 1.9–40 nm with a maximum at about 2.7 nm. As shown in Table 1, the average pore diameter and pore volume decrease with the loading of iron, because iron particles clogged some pores during the catalyst preparation. TEM image (Figure 2) also shows that some metal particles entered the pipelines of CNTs. The specific surface area of the catalysts exhibited a unique trend with the increase of K content, which first increased to 177.1 m<sup>2</sup>/g due to the improved dispersion of microcrystalline particles and the reduced particle size, following decrease to 156.2 m<sup>2</sup>/g owing to the K monomer layer generated on the iron surface. This phenomenon has been certified by You et al.<sup>[38]</sup>

### 3.3 | Thermogravimetric analysis of the catalysts

The results of TG/DTG in air were used to indicate the thermal stability of the catalysts. The effect of potassium on the thermal stability of the catalysts was revealed by initial weight loss temperature and oxidation temperature. It can be seen from Figure 4 that with the increase of K content, initial weight loss temperature and oxidation temperature of the catalysts decrease from 337 and

454 °C to 306 and 423 °C, respectively, which indicates that K has a certain catalytic effect on the oxidation of the carrier because of the increased defect sites on CNT surface. The iron loading of the catalysts could be calculated by the residual mass fraction from the thermogravimetric analysis results. As shown in the picture, the weight loss rates of all Fe-xK/CNT catalysts are around 70 wt.%, whereas the support is nearly 100%. Iron species would eventually convert to α-Fe<sub>2</sub>O<sub>3</sub> when the temperature was higher than 350 °C.<sup>[41]</sup> The final mass fraction of these five catalysts is about 30 wt.%, so the actual loading of iron is roughly equal to the theoretical loading of about 20 wt.%.

### 3.4 | Raman analysis of the catalysts

Raman spectroscopy was used to investigate the defects and the graphitization degree on carbon materials. As shown in Figure 5, the relative intensity of the D-band and the G-band ( $I_D/I_G$ ) increases distinctly from 1.08 to 1.17 with the addition of K. The D-band at about 1345 cm<sup>-1</sup> corresponded to the disordered graphitic lattice, and another peak at 1575 cm<sup>-1</sup> was the G-band representing the graphitic carbon structure,<sup>[42]</sup> and a higher ratio of  $I_D/I_G$  meant more defects on the sample.<sup>[43,44]</sup> The increased value of  $I_D/I_G$  reveals that K promotes the formation of defects among the CNT surface. This consequence also explains that the addition of K reduced the oxidation temperature of the catalyst in the TG characterization. Abbaslou<sup>[45]</sup> proved that the more defects on CNT surface resulted in smaller metal particles and stronger metal-carrier interaction. Besides, the carbon

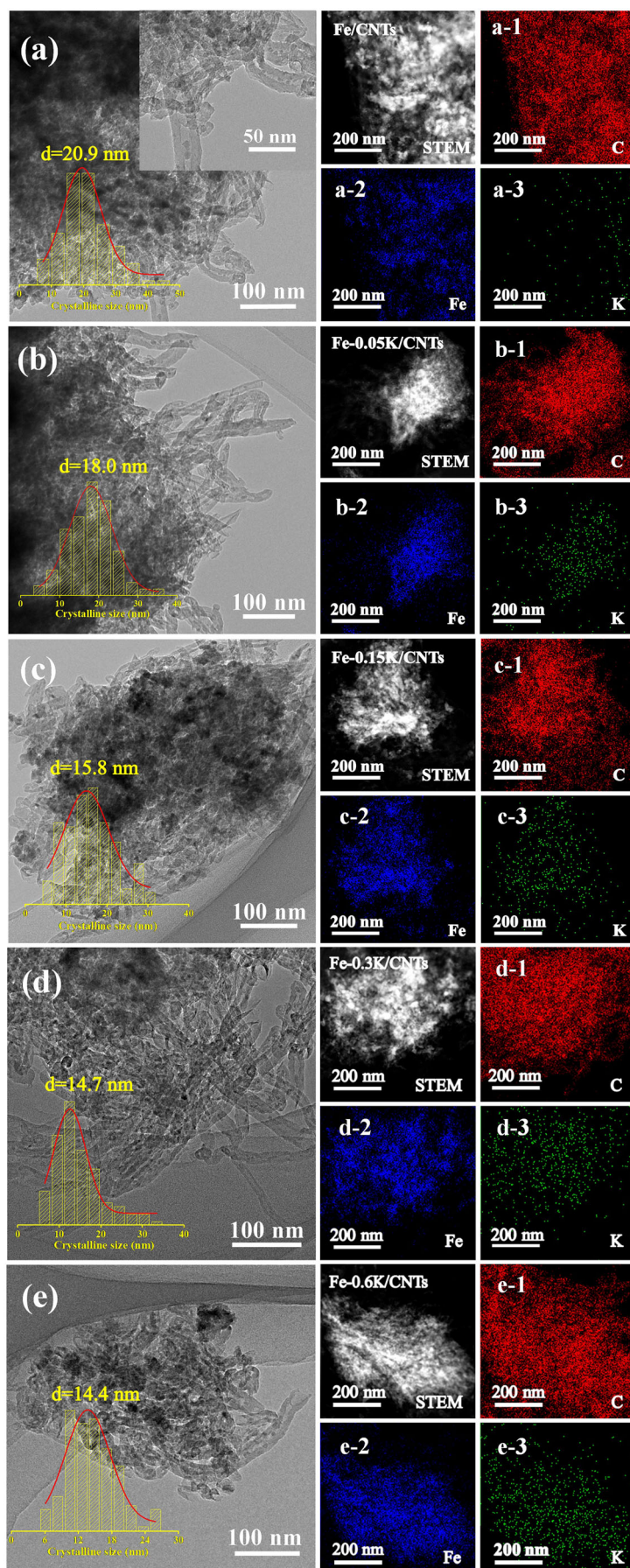


FIGURE 2 TEM images (a–e); STEM images and EDX-mapping of Fe/CNTs (a), Fe-0.05K/CNTs (b), Fe-0.15K/CNTs (c), Fe-0.3K/CNTs (d), Fe-0.6K/CNTs (e)

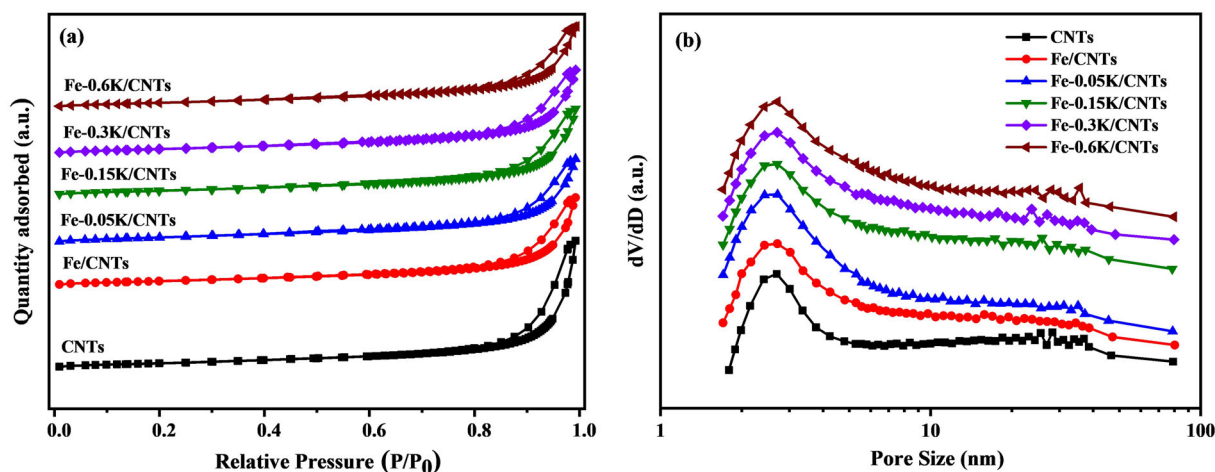
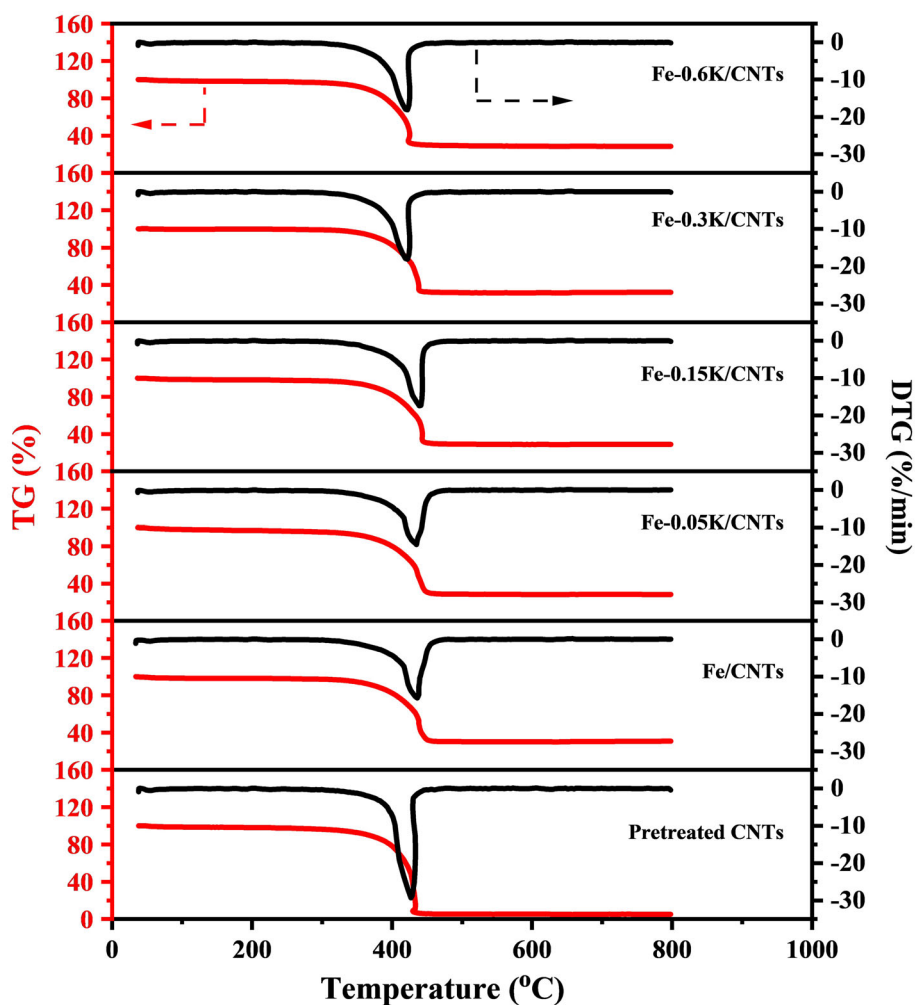


FIGURE 3 N<sub>2</sub> adsorption–desorption isotherms (a) and pore size distribution (b) of Fe-xK/CNT catalysts and support

FIGURE 4 TG and DTG profiles of Fe-xK/CNT catalysts and support



support with a high graphitization degree had stronger electron transfer capability, which could facilitate the CO activation.<sup>[46]</sup> Therefore, adding excessive K promoter may inhibit the transformation of intermediate CO.

### 3.5 | Reduction behavior of the catalysts

As shown in Figure 6, the H<sub>2</sub>-TPR profiles of all catalysts have three major reduction peaks, which are

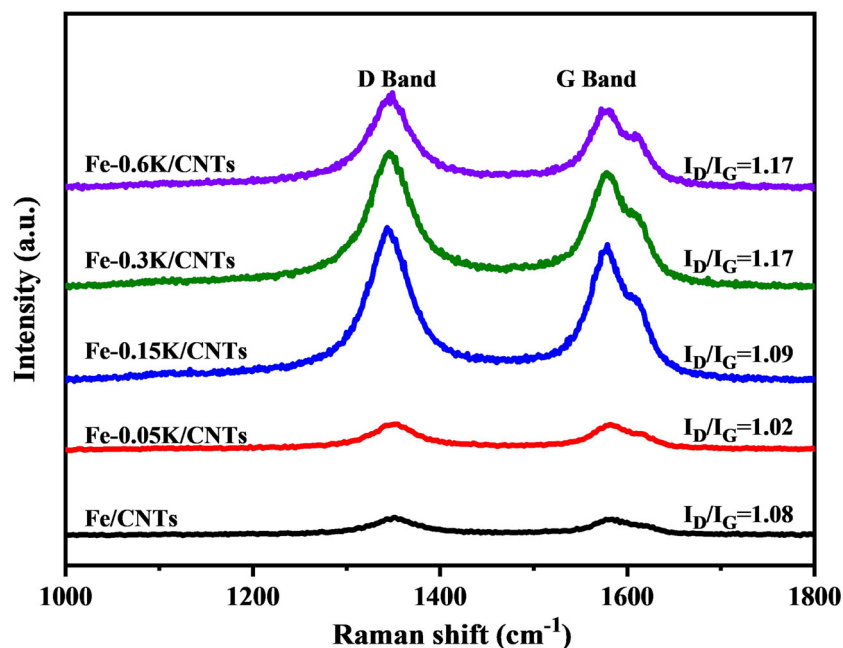


FIGURE 5 Raman spectra of Fe-xK/CNT catalysts

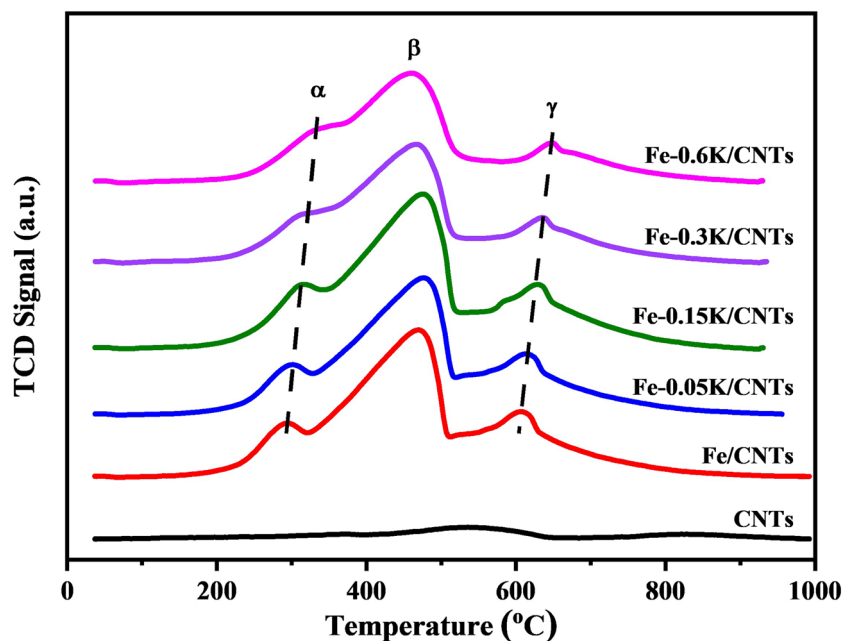


FIGURE 6 H<sub>2</sub>-TPR profiles of Fe-xK/CNT catalysts and support

located at 290–320 °C, 350–500, and 500–650 °C, respectively. The first peak could be attributed to the reduction of Fe<sub>2</sub>O<sub>3</sub> to Fe<sub>3</sub>O<sub>4</sub>, and the last two peaks accounted for the reduction process of magnetite, in which Fe<sub>3</sub>O<sub>4</sub> was reduced to FeO and then to metallic Fe.<sup>[47–49]</sup> Upon increasing the potassium loading, peak  $\alpha$  and peak  $\gamma$  both have a progressive shift to higher temperatures, indicating that the reducibility of these five catalysts was retarded by the potassium. The temperature of the peak  $\beta$  appears non-monotonic change with the increase of K content, which was caused by

the interaction between iron oxide and potassium oxide. A small amount of K slightly inhibited the reduction of Fe<sub>3</sub>O<sub>4</sub>, but excessive K facilitated the reduction process, which was also discovered by Xiong et al.<sup>[37]</sup> It means that K addition inhibited the reduction of Fe<sub>2</sub>O<sub>3</sub> but promoted the reduction process of Fe<sub>3</sub>O<sub>4</sub> to metallic Fe.<sup>[50]</sup> The area of the reduction peaks decreases significantly with the addition of potassium because the alkaline metals hindered the consumption of hydrogen, which suggests that the K decreased the reduction degree of the catalysts.

### 3.6 | XPS of the catalysts

The chemical state of the elements in calcined catalysts was tested by X-ray photoelectron spectroscopy (XPS) as shown in Figure 7; the scanned XPS spectra of all catalysts present an analogous trend (Figure 7a). It can be seen from Figure 7b that the ratio of  $sp^2/sp^3$  on C 1 s peak of the Fe-xK/CNT catalysts decreases with the addition of K, which represents that the addition of potassium increases the defects on surface of CNTs.

Fe 2p occurs spin-orbit splitting and has the two main peaks at the binding energies of 711.4 and 725.1 eV in Figure 7c, in which they correspond to the Fe  $2p_{3/2}$  and Fe  $2p_{1/2}$  of  $Fe^{3+}$ , respectively. All catalysts exhibited the typical spectra for  $Fe_2O_3$  with a satellite peak at 718.5–719.3 eV, so the iron species in the catalysts mainly existed as  $Fe_2O_3$ .<sup>[51]</sup> In addition, Fe  $2p_{3/2}$  can be divided into three peaks with the binding energy of 710.3, 711.4, and 713.1 eV, and the ratios of the  $Fe^{2+}$  and  $Fe^{3+}$  calculated by Fe  $2p_{3/2}$  peak areas are listed in Table 2. The

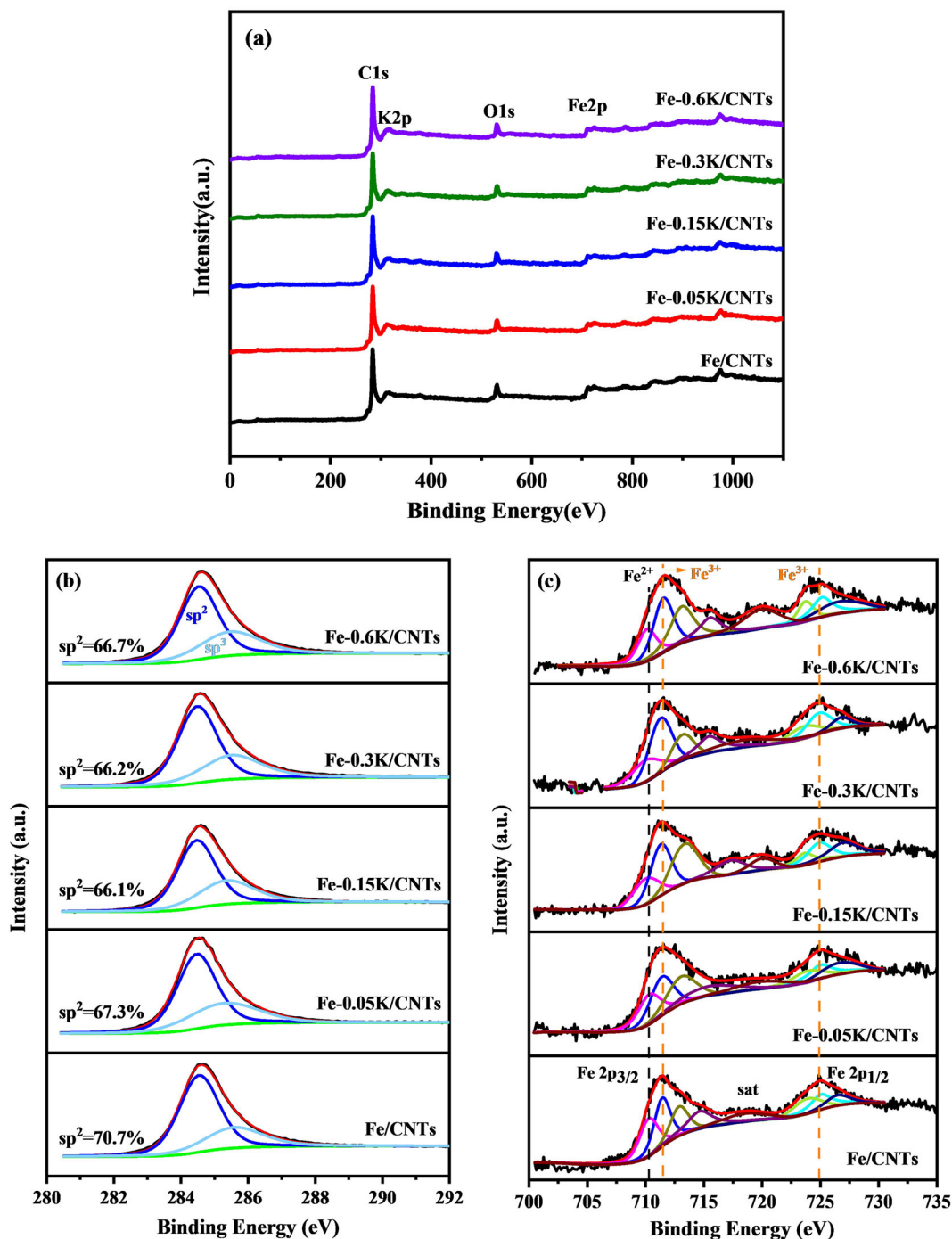


FIGURE 7 Scanned XPS spectra (a) and high-resolution C 1 s (b), Fe 2p (c) of different catalysts

**TABLE 2** XPS analysis results and parameters of the catalysts for Fe 2P<sub>3/2</sub> spectra

Sample	Fe 2P <sub>3/2</sub>			Fe <sub>2+</sub> /Fe <sub>3+</sub> <sup>a</sup>
	BE (eV)	A (area)	A%	
Fe/CNTs	711.6	5492.1	39.2	0.89
	710.5	4892.7	35.0	
	713.1	3612.2	25.8	
Fe-0.05K/CNTs	711.7	4081.6	35.9	0.88
	710.6	3598.9	31.7	
	713.4	3684.7	32.4	
Fe-0.15K/CNTs	711.5	5303.7	39.2	0.58
	710.3	3068.6	22.7	
	713.6	5171.6	38.2	
Fe-0.3K/CNTs	711.1	5310.9	45.6	0.59
	709.7	39,571	34.0	
	712.9	2368.1	20.4	
Fe-0.6K/CNTs	711.7	5291.2	39.9	0.61
	710.3	3224.2	24.3	
	713.3	4753.9	35.8	

<sup>a</sup>This value is obtained by the area of peak at BE = 710.5 divided by the area at BE = 711.6.

value of Fe<sup>2+</sup>/Fe<sup>3+</sup> in the octahedral structure decreased with the addition of K, demonstrating that the reducibility of catalysts was correspondingly reduced, which is consistent with the increased reduction temperature in H<sub>2</sub>-TPR.

### 3.7 | Catalytic activity

In order to understand the effects of potassium promoter on the performance of Fe-xK/CNT catalysts, the activity of Fe-1K/CNT catalyst with excessive potassium was also tested. The catalytic activity and product selectivity of these six catalysts are shown in Figure 8. Both CO<sub>2</sub> conversion and C<sub>2-4</sub> selectivity are improved as K/Fe ratio increases from 0 to 0.05. Further increase of K/Fe ratio slightly reduces the CO<sub>2</sub> conversion and drastically decreases C<sub>2-4</sub> selectivity. The potassium content significantly affects the selectivity to CH<sub>4</sub> and long-chain hydrocarbons. CH<sub>4</sub> selectivity decreases from 31% to about 12%, whereas there is little change when the molar ratio was higher than 0.3. C<sub>5+</sub> selectivity exhibits an opposite tendency to that of CH<sub>4</sub>; it rises to 56% with ascending K/Fe ratio to 0.3 and then maintains at about 55%.

Compared with the unpromoted Fe/CNT catalyst, adding a small amount of potassium to the catalysts resulted in higher CO<sub>2</sub> conversion and C<sub>5+</sub> selectivity,

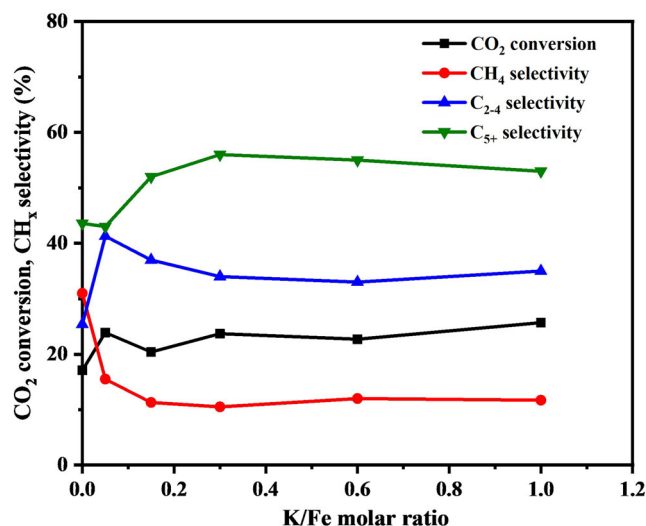


**FIGURE 8** Effect of K/Fe molar ratio on activity of the Fe-xK/CNT catalysts for CO<sub>2</sub> hydrogenation

but a large amount of K showed a negative effect on activity. Furthermore, as the molar ratio of K/Fe was greater than 0.3, both activity and C<sub>5+</sub> selectivity changed a little with the further increase of potassium content. According to the CO<sub>2</sub>-TPD results in Table 1, the addition of potassium enhanced the surface alkalinity of the catalysts, which accelerated the CO<sub>2</sub> chemisorption and led to an increase of CO<sub>2</sub> conversion. A high CO<sub>2</sub> conversion provided more CO species for subsequent FTS, thus promoting the synthesis of hydrocarbons. And the increased CO species promoted the carburization of iron, thereby enhancing the activity of the catalysts for CO<sub>2</sub> hydrogenation. This result is consistent with the findings of Visconti.<sup>[52]</sup> According to the results of XRD and TEM, the particle size of iron species reduced upon the addition of K that facilitates the access of the reactants to the active phase. However, excess K-doping reduced the activity due to the decreased CO<sub>2</sub> chemisorption.

The activity results indicate that the Fe/CNT catalyst with K-loading achieved higher C<sub>5+</sub> selectivity, but excessive potassium showed little effect on it. We deduce that the effect of K on the selectivity of long-chain hydrocarbons is from the compromising effect of K on CO<sub>2</sub> chemisorption, reduction degree, and graphitization degree of catalysts. CO<sub>2</sub>-TPD results show that the amount of CO<sub>2</sub> chemisorption increased first and then decreased on the Fe-xK/CNT catalysts. As reported, K as a promoter of iron-based catalysts facilitated the adsorption of CO and CO<sub>2</sub> and inhibited H<sub>2</sub> adsorption, which decreased the H/C ratio on the catalysts surface, thus promoting the carburization of the iron species and increasing the possibility of chain growth.<sup>[53,54]</sup> Therefore, the product distribution shifted to high molecular weight hydrocarbons. In

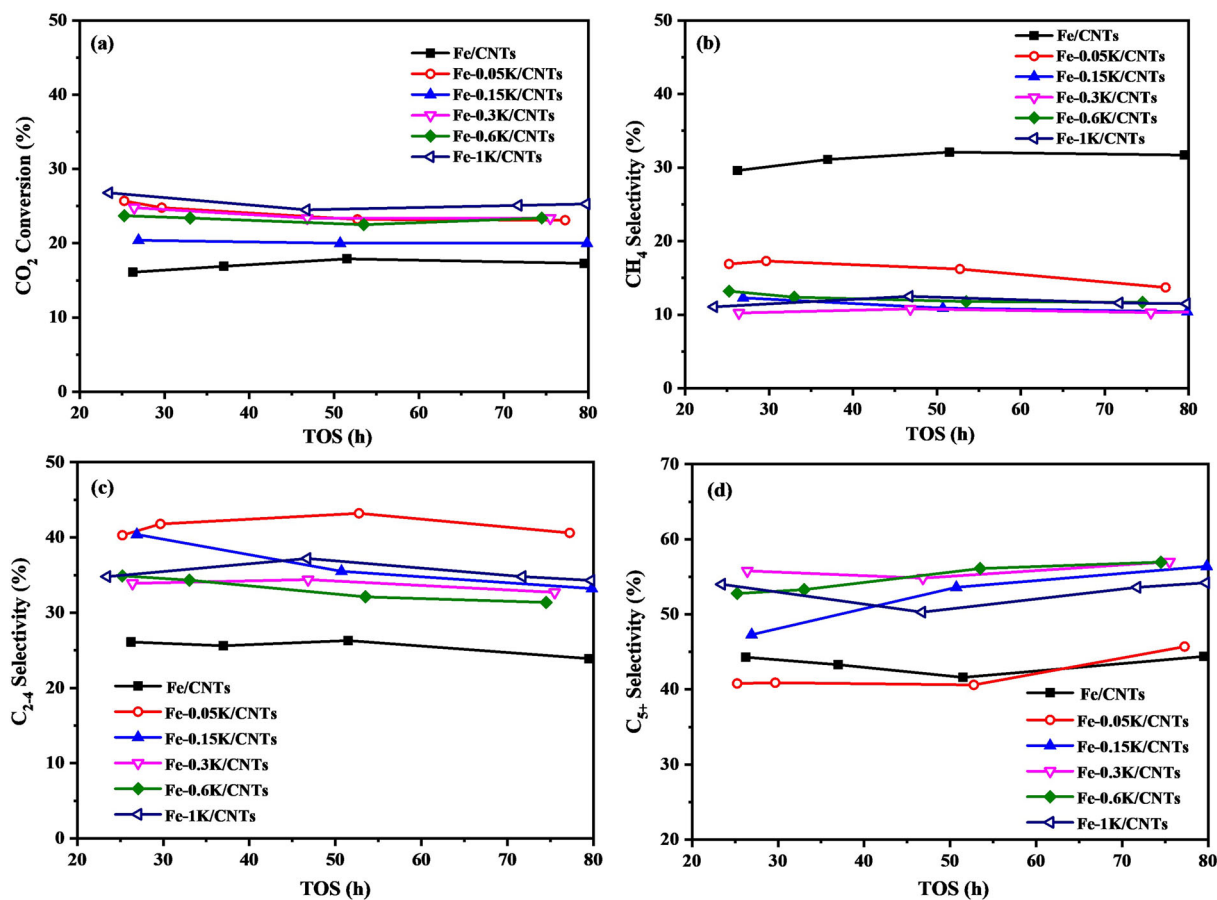


FIGURE 9 CO<sub>2</sub> conversion and product selectivity for CO<sub>2</sub> hydrogenation reaction

particular, K could promote the formation of vacancies on the surface of iron oxides and iron carbides, which were used as active sites for RWGS and FTS reactions, respectively.<sup>[15]</sup> Besides, the long-range ordered structure of CNTs contributed to the aggregation of the reaction intermediate. The reaction intermediate trapped in the channels of CNTs might get longer contact time with the iron species, which is conducive to the growth of long-chain hydrocarbons.<sup>[33]</sup> In another respect, the previous morphological properties of catalysts (Table 1) and H<sub>2</sub>-TPR results (Figure 6) evidence that excess K decreased the specific surface area and reduction degree of the catalyst, thus impeding the chemisorption and activation of CO<sub>2</sub>. Furthermore, potassium increased the local defects of CNTs, which reduced the graphitization degree and impeded the transformation of CO intermediate because the graphitization degree of carbon materials was positively related to CO conversion.<sup>[29,46]</sup> Due to the compromising effects of K on the properties of the catalyst, there is a suitable amount of K/Fe ratio that is found to be 0.3. The Fe-0.3K/CNT catalyst exhibits the highest C<sub>5+</sub> selectivity and the lowest CH<sub>4</sub> selectivity.

Furthermore, the long-term stability data of the K-modified Fe/CNTs are essential; the variation in CO<sub>2</sub> conversion and product selectivity versus time are shown in Figure 9. The K-doped Fe/CNT catalyst remains unchanged during 60 h, which proves that the stability of Fe-xK/CNT catalysts is good.

## 4 | CONCLUSION

The effects of potassium on the specific surface area, acid-base property, reduction behavior, and CO<sub>2</sub> chemisorption on the Fe-xK/CNT catalysts were investigated. The addition of potassium enhanced the CO<sub>2</sub> conversion and C<sub>5+</sub> selectivity because of the increased alkalinity and decreased iron oxide particle size on the catalyst surface. But over-doping K suppressed the chemisorption of CO<sub>2</sub> and the formation of C<sub>5+</sub> hydrocarbons due to the decreased reduction degree, specific surface area, and graphitization degree of the catalyst. The catalyst with a K/Fe molar ratio of 0.3 achieved the optimum performance of CO<sub>2</sub> hydrogenation.

## ACKNOWLEDGMENTS

We appreciate the financial support by the Joint Funds of the National Natural Science Foundation of China (Grant No. U20A20124) and the Program of Introducing Talents of Discipline to Universities (No. BP0618007).

## AUTHOR CONTRIBUTIONS

**Liya Dai:** Data curation; formal analysis. **Yao Chen:** Formal analysis; methodology. **Renjie Liu:** Investigation; methodology. **Xin Li and Niamat Ullah:** Review & editing. **Zhenhua Li:** Funding acquisition; supervision.

## CONFLICT OF INTEREST

No conflict of interest exists in the submission of this manuscript, and the manuscript is approved by all authors for publication.

## DATA AVAILABILITY STATEMENT

The data supporting the findings of this study are available within the article.

## ORCID

Liya Dai  <https://orcid.org/0000-0002-8266-8906>

Yao Chen  <https://orcid.org/0000-0002-3715-6565>

Renjie Liu  <https://orcid.org/0000-0002-7146-0149>

Xin Li  <https://orcid.org/0000-0002-6658-6003>

Niamat Ullah  <https://orcid.org/0000-0002-5235-8472>

Zhenhua Li  <https://orcid.org/0000-0002-4101-2767>

## REFERENCES

- [1] F. Jiang, B. Liu, S. S. Geng, Y. B. Xu, X. H. Liu, *Cat. Sci. Technol.* **2018**, *8*, 4097.
- [2] F. Song, Q. Zhong, Y. Zhao, *Appl. Organomet. Chem.* **2015**, *29*, 612.
- [3] Y. Abdoli, M. Razavian, S. Fatemi, *Appl. Organomet. Chem.* **2019**, *33*(8).
- [4] G. Centi, S. Perathoner, *Catal. Today* **2009**, *148*, 191.
- [5] C. G. Visconti, M. Martinelli, L. Falbo, L. Fratolocchi, L. Lietti, *Catal. Today* **2016**, *277*, 161.
- [6] T. Numpilai, N. Chanlek, Y. Poo-Arporn, C. K. Cheng, N. Siri-Nguan, T. Sornchamni, M. Chareonpanich, P. Kongkachuichay, N. Yigit, G. Rupprechter, J. Limtrakul, T. Witoon, *Chem. Cat. Chem.* **2020**, *12*, 3306.
- [7] W. S. Ning, B. Li, B. Wang, X. Z. Yang, Y. F. Jin, *Catal. Lett.* **2019**, *149*, 431.
- [8] S. M. Hwang, C. Zhang, S. J. Han, H. G. Park, Y. T. Kim, S. Yang, K. W. Jun, S. K. Kim, *J. CO<sub>2</sub> Util.* **2020**, *37*, 65.
- [9] M. Albrecht, U. Rodemerck, M. Schneider, M. Bröring, D. Baabe, E. V. Kondratenko, *Appl. Catal. B-Environ.* **2017**, *204*, 119.
- [10] S. Saeidi, N. A. S. Amin, M. R. Rahimpour, *J. CO<sub>2</sub> Util.* **2014**, *5*, 66.
- [11] G. M. Iglesias, C. de Vries, M. Claeys, G. Schaub, *Catal. Today* **2015**, *242*, 184.
- [12] W. Li, A. Zhang, X. Jiang, M. J. Janik, J. Qiu, Z. Liu, X. Guo, C. Song, *J. CO<sub>2</sub> Util.* **2018**, *23*, 219.
- [13] T. Numpilai, T. Witoon, N. Chanlek, W. Limphirat, G. Bonura, M. Chareonpanich, J. Limtrakul, *Appl. Catal. A. Gen.* **2017**, *547*, 219.
- [14] F. C. F. Marcos, J. M. Assaf, E. M. Assaf, *Mol. Catal.* **2018**, *458*, 297.
- [15] M. Amoyal, R. Vidruk-Nehemya, M. V. Landau, M. Herskowitz, *J. Catal.* **2017**, *348*, 29.
- [16] S. S. Nam, G. Kishan, M. W. Lee, M. J. Choi, K. W. Lee, *Appl. Organomet. Chem.* **2000**, *14*, 794.
- [17] N. A. M. Razali, K. T. Lee, S. Bhatia, A. R. Mohamed, *Renew. Sustain. Energy Rev.* **2012**, *16*, 4951.
- [18] W. Li, H. Wang, X. Jiang, J. Zhu, Z. Liu, X. Guo, C. Song, *RSC Adv.* **2018**, *8*, 7651.
- [19] F. Ding, A. Zhang, M. Liu, Y. Zuo, K. Li, X. Guo, C. Song, *Ind. Eng. Chem. Res.* **2014**, *53*, 17563.
- [20] T. Xie, J. Wang, F. Ding, A. Zhang, W. Li, X. Guo, C. Song, *J. CO<sub>2</sub> Util.* **2017**, *19*, 202.
- [21] N. Boreriboon, X. Jiang, C. Song, P. Prasassarakich, *J. CO<sub>2</sub> Util.* **2018**, *25*, 330.
- [22] L. M. Chew, P. Kangvansura, H. Ruland, H. J. Schulte, C. Somsen, W. Xia, G. Eggeler, A. Worayingyong, M. Muhler, *Appl. Catal. A. Gen.* **2014**, *482*, 163.
- [23] A. Dokania, A. D. Chowdhury, A. Ramirez, S. Telalovic, E. Abou-Hamad, L. Gevers, J. Ruiz-Martinez, J. Gascon, *J. Catal.* **2020**, *381*, 347.
- [24] J. Liu, Y. Sun, X. Jiang, A. Zhang, C. Song, X. Guo, *J. CO<sub>2</sub> Util.* **2018**, *25*, 120.
- [25] V. G. Komvokis, S. Karakoulia, E. F. Iliopoulou, M. C. Papapetrou, I. A. Vasalos, A. A. Lappas, K. S. Triantafyllidis, *Catal. Today* **2012**, *196*, 42.
- [26] S. Abello, D. Montane, *Chem. Sus. Chem.* **2011**, *4*, 1538.
- [27] Z. Li, R. Liu, Y. Xu, X. Ma, *Appl. Surf. Sci.* **2015**, *347*, 643.
- [28] M. C. Bahome, L. L. Jewell, D. Hildebrandt, D. Glasser, *Appl. Catal. A. Gen.* **2005**, *287*, 60.
- [29] T. Fu, R. Liu, J. Lv, Z. Li, *Fuel Process. Technol.* **2014**, *122*, 49.
- [30] X. Zhao, S. Lv, L. Wang, L. Li, G. Wang, Y. Zhang, J. Li, *Mol. Catal.* **2018**, *449*, 99.
- [31] A. N. Andriotis, M. Menon, G. E. Froudakis, *Chem. Phys. Lett.* **2000**, *320*, 425.
- [32] F. Zhao, H. Duan, W. Wang, J. Wang, *Phys. B* **2012**, *407*, 2495.
- [33] W. Chen, Z. Fan, X. Pan, X. Bao, *J. Am. Chem. Soc.* **2008**, *130*, 9414.
- [34] P. Kangvansura, L. M. Chew, W. Saengsui, P. Santawaja, Y. Poo-arporn, M. Muhler, H. Schulz, A. Worayingyong, *Catal. Today* **2016**, *275*, 59.
- [35] G. Zhao, C. Zhang, S. Qin, H. Xiang, Y. Li, *J. Mol. Catal. A: Chem.* **2008**, *286*, 137.
- [36] Y. Yang, H. W. Xiang, Y. Y. Xu, L. Bai, Y. W. Li, *Appl. Catal. A. Gen.* **2004**, *266*, 181.
- [37] H. Xiong, M. A. Motchelaho, M. Moyo, L. L. Jewell, N. J. Coville, *Fuel* **2015**, *150*, 687.
- [38] Z. You, W. Deng, Q. Zhang, Y. Wang, *Chin. J. Catal.* **2013**, *34*, 956.
- [39] P. Kangvansura, L. M. Chew, C. Kongmark, P. Santawaja, H. Ruland, W. Xia, H. Schulz, A. Worayingyong, M. Muhler, *Engineering* **2017**, *3*, 385.

- [40] S. L. Soled, E. Iglesia, S. Miseo, B. A. DeRites, R. A. Fiato, *Top. Catal* **1995**, *2*, 193.
- [41] M. Stefanescu, O. Stefanescu, C. Lazau, *J. Therm. Anal. Calorim.* **2007**, *88*, 27.
- [42] S. Maldonado, S. Morin, K. J. Stevenson, *Carbon* **2006**, *44*, 1429.
- [43] R. Liu, R. Liu, X. Ma, B. H. Davis, Z. Li, *Fuel* **2018**, *211*, 827.
- [44] P. V. Shanahan, L. Xu, C. Liang, M. Waje, S. Dai, Y. S. Yan, J. Power, *Sources* **2008**, *185*, 423.
- [45] R. M. Malek Abbaslou, A. Tavasoli, A. K. Dalai, *Appl. Catal. A. Gen.* **2009**, *355*, 33.
- [46] Z. Fan, W. Chen, X. Pan, X. Bao, *Catal. Today* **2009**, *147*, 86.
- [47] Q. Chen, G. Liu, S. Ding, M. Chanmiya Sheikh, D. Long, Y. Yoneyama, N. Tsubaki, *Chem. Eng. J.* **2018**, *334*, 714.
- [48] J. D. Xu, K. T. Zhu, X. F. Weng, W. Z. Weng, C. J. Huang, H. L. Wan, *Catal. Today* **2013**, *215*, 86.
- [49] J. Lu, L. Yang, B. Xu, Q. Wu, D. Zhang, S. Yuan, Y. Zhai, X. Wang, Y. Fan, Z. Hu, *ACS Catal.* **2014**, *4*, 613.
- [50] S. R. Yan, K. W. Jun, J. S. Hong, M. J. Choi, K. W. Lee, *Appl. Catal. A. Gen.* **2000**, *194*, 63.
- [51] T. Numpilai, N. Chanlek, Y. Poo-Arporn, S. Wannapaiboon, C. K. Cheng, N. Siri-Nguane, T. Sornchamni, P. Kongkachuichay, M. Chareonpanich, G. Rupprechter, J. Limtrakul, T. Witoon, *Appl. Surf. Sci.* **2019**, *483*, 581.
- [52] C. G. Visconti, M. Martinelli, L. Falbo, A. Infantes-Molina, L. Liettia, P. Forzatti, G. Iaquaniello, E. Palo, B. Picutti, F. Brignoli, *Appl. Catal. Environ.* **2017**, *200*, 530.
- [53] D. Mattia, M. D. Jones, J. P. O'Byrne, O. G. Griffiths, R. E. Owen, E. Sackville, M. McManus, P. Plucinski, *Chem. Sus. Chem.* **2015**, *8*, 4064.
- [54] W. D. Shafer, G. Jacobs, U. M. Graham, H. H. Hamdeh, B. H. Davis, *J. Catal.* **2019**, *369*, 239.

**How to cite this article:** Dai L, Chen Y, Liu R, Li X, Ullah N, Li Z. CO<sub>2</sub> hydrogenation to C<sub>5+</sub> hydrocarbons over K-promoted Fe/CNT catalyst: Effect of potassium on structure–activity relationship. *Appl Organomet Chem.* 2021;e6253. <https://doi.org/10.1002/aoc.6253>